



HAL
open science

Effect of Ag Doping on Electronic Structure of Cluster Compounds $\text{Ag}_x\text{Mo}_9\text{Se}_{11}$ ($x = 3.4, 3.9$)

Sergei M. Butorin, Kristina Kvashnina, Mattias Klintenber, Matjaž Kavčič, Matjaž Žitnik, Klemen Bučar, Patrick Gougeon, Philippe Gall, Christophe Candolfi, Bertrand Lenoir

► **To cite this version:**

Sergei M. Butorin, Kristina Kvashnina, Mattias Klintenber, Matjaž Kavčič, Matjaž Žitnik, et al.. Effect of Ag Doping on Electronic Structure of Cluster Compounds $\text{Ag}_x\text{Mo}_9\text{Se}_{11}$ ($x = 3.4, 3.9$). ACS Applied Energy Materials, 2018, 1 (8), pp.4032-4039. 10.1021/acsaem.8b00718 . hal-01969359

HAL Id: hal-01969359

<https://hal.science/hal-01969359>

Submitted on 7 Mar 2023

HAL is a multi-disciplinary open access archive for the deposit and dissemination of scientific research documents, whether they are published or not. The documents may come from teaching and research institutions in France or abroad, or from public or private research centers.

L'archive ouverte pluridisciplinaire **HAL**, est destinée au dépôt et à la diffusion de documents scientifiques de niveau recherche, publiés ou non, émanant des établissements d'enseignement et de recherche français ou étrangers, des laboratoires publics ou privés.

Effect of Ag doping on electronic structure of cluster compounds $\text{Ag}_x\text{Mo}_9\text{Se}_{11}$ ($x=3.4; 3.9$)

S. M. Butorin,¹ K. O. Kvashnina,^{2,3} M. Klintonberg,¹ M. Kavčič,⁴ M. Žitnik,^{4,5} K. Bučar,⁴ P. Gougeon,⁶ P. Gall,⁶ C. Candolfi,⁷ and B. Lenoir⁷

¹*Department of Physics and Astronomy, Uppsala University, P. O. Box 516, SE-751 20 Uppsala, Sweden*

²*The European Synchrotron, CS40220, 38043 Grenoble Cedex 9, France*

³*Helmholtz-Zentrum Dresden-Rossendorf (HZDR),*

Institute of Resource Ecology, P.O. Box 510119, 01314, Dresden, Germany

⁴*Jožef Stefan Institute, Jamova cesta 39, SI-1001 Ljubljana, Slovenia*

⁵*Faculty of Mathematics and Physics, University of Ljubljana, Jadranska ulica 19, Ljubljana, Slovenia*

⁶*Institut des Sciences Chimiques de Rennes, UMR 6226 CNRS - Université de Rennes 1 - INSA de Rennes, 11 allée de Beaulieu, CS 50837, 35708 Rennes Cedex, France*

⁷*Institut Jean Lamour, UMR 7198 CNRS-Université de Lorraine, Parc de Saurupt, CS 50840, F-54011 Nancy, France*

The electronic structure of $\text{Ag}_x\text{Mo}_9\text{Se}_{11}$ as potential material for thermoelectric applications was studied using high-energy-resolution fluorescence-detection x-ray absorption spectroscopy (HERFD-XAS) and resonant inelastic x-ray scattering (RIXS) technique. The experiments were supported by first-principle calculations using density functional theory (DFT). The analysis of obtained spectra indicate the presence of subvalent (less than 1+) Ag in the $\text{Ag}_x\text{Mo}_9\text{Se}_{11}$. The advanced HERFD-XAS measurements allowed us to resolve the contribution of the electronic states at the Fermi level of $\text{Ag}_x\text{Mo}_9\text{Se}_{11}$ and monitor its dependence on the x value. Comparison of the experimental data with the results of the DFT calculations suggests an importance of the Ag2-type sites with the shortest Ag-Se distance for affecting the properties of $\text{Ag}_x\text{Mo}_9\text{Se}_{11}$.

I. INTRODUCTION

Chevrel-phase related compounds¹ have become known for their superconducting properties. Ternary chalcogenides, such as $\text{M}_x\text{Mo}_6\text{Q}_8$, where Q = S, Se, Te and M can be simple or transition metal or rare-earth, exhibit superconducting transition temperatures ranging up to 15 K with high critical magnetic fields.^{2,3} The Mo_6 cluster compounds have also turned to be a good material for producing the quasi-1D superconductors⁴⁻⁶ and some of the Mo_6 -based compounds have been recently shown to exhibit interesting topological properties.⁷ Compounds with Mo clusters with nuclearity ranging up to 36 (Ref.⁸) have been synthesized and besides the studies of their superconducting properties, the research efforts have been made to assess thermoelectric properties of the Mo-cluster materials.⁹⁻¹¹

Recently, the dimensionless thermoelectric figure of merit ZT of ~ 0.65 was found for $\text{Ag}_x\text{Mo}_9\text{Se}_{11}$ ($x=3.8$ or 3.9) at 800 K (Refs.¹²⁻¹⁴) which is a significant improvement over the best previously known value in the Chevrel phase family. For this $\text{Ag}_x\text{Mo}_9\text{Se}_{11}$ system, the low thermal conductivity, comparable to values observed in state-of-the-art thermoelectric materials, was obtained. While such low thermal conductivity was assumed to be due to the strong disorder induced by the Ag atoms combined with their high ability to vibrate about their equilibrium positions, it is not really clear how the Ag doping affects the electronic structure of the system. The reported density functional theory (DFT) calculations of the electronic structure of $\text{Ag}_x\text{Mo}_9\text{Se}_{11}$ predict the rigid-band model behavior when the Ag content varies¹⁴ but some experimental data, such as the results of the spe-

cific heat measurements,¹⁴ indicate that the rigid-band approximation¹⁵ may not be fully applicable for this system.

The validity of the the rigid-band approximation, which is often used in calculating the thermopower in doped narrow band semiconductors, has been discussed with respect to potential materials for thermoelectric applications, such as selenides, tellurides and half-Heusler compounds, in a number of publications (see Refs.¹⁶⁻¹⁹ and references therein). However, there is no consensus on the extent of the applicability of this approximation.

In our study, we employed the advanced x-ray spectroscopic techniques, such as high energy resolution fluorescence detection (HERFD) mode of x-ray absorption spectroscopy (XAS) and resonant inelastic x-ray scattering (RIXS) to probe the electronic structure of the $\text{Ag}_x\text{Mo}_9\text{Se}_{11}$ system. The experiments were also supported by DFT calculations and the results are not in favor of the rigid-band model behavior. The improved resolution of the HERFD-XAS compared to conventional XAS allowed us to not only more efficiently study the chemical state of inserted Ag in $\text{Ag}_x\text{Mo}_9\text{Se}_{11}$ but to resolve the structures in the spectra of the Ag L_2 and Se K edges corresponding to the contributions of the unoccupied Ag and Se states at the Fermi level in $\text{Ag}_x\text{Mo}_9\text{Se}_{11}$ and to monitor their changes with varying x .

II. EXPERIMENTAL METHODS

The samples used in the present work were the same as those used for low-temperature transport properties measurements in Ref.¹⁴. The two polycrystalline

$\text{Ag}_x\text{Mo}_9\text{Se}_{11}$ samples with nominal compositions $x = 3.4$ and 3.9 were synthesized in an argon-filled glove box. In a first step, the binary MoSe_2 was synthesized from Mo (99.999%) and Se (99.999%) powders in a sealed, evacuated silica ampule heated at 800°C for 48 h. Prior to use, Mo powder was heated under H_2 flowing gas at 1000°C for ten hours to eliminate possible traces of oxygen. The $\text{Ag}_x\text{Mo}_9\text{Se}_{11}$ compounds were synthesized from stoichiometric amounts of elemental Ag (99.999%), Mo and MoSe_2 powders sealed in evacuated silica tubes and heated at 950° for 48 h. The ingots were ground into micron-sized powders and densified by spark plasma sintering at 1050° under a uniaxial pressure of 80 MPa during 10 min. The relative density of the pellets was determined to be above 95% for both samples.

Powder X-ray diffraction patterns were recorded by using a Bruker D8 Advance diffractometer ($\text{Cu } K\alpha_1$ radiation; $\lambda = 1.5406 \text{ \AA}$). Both samples crystallize in the orthorhombic space group $Cmcm$, in agreement with single-crystal data. Electron probe microanalysis was used to determine the actual chemical composition for each samples. While a good correlation between the nominal and actual compositions was found for the $x = 3.4$ sample (actual $x = 3.41$), these analyses revealed that the actual Ag content is slightly lower ($x = 3.71$) than the nominal one in the $x = 3.9$ sample. Hereafter, the samples will be labeled by their actual Ag contents.

The spectroscopic measurements were performed at beamline ID26 of the European Synchrotron in Grenoble.²⁰ The incident photon energies were selected using a double Si(111) crystal monochromator. Higher harmonics were suppressed by two Si mirrors operating in total reflection. The photon beam was focused down to $50 \times 250 \mu\text{m}^2$ and directed on a sample, the directions of the incident and emitted photons were 45° relative to the sample surface.

The XAS spectra were measured in the HERFD mode using an Johann type point-to-point focusing x-ray emission spectrometer.²¹ The sample, crystal analyzer and avalanche photodiode detector were positioned on the vertical Rowland circle of 1 m diameter. The Ag HERFD spectra at the L_2 edge were obtained by recording the maximum intensity of the Ag $L\beta_1$ ($2p_{1/2} - 3d_{3/2}$ transition) x-ray emission line at $\sim 3150.5 \text{ eV}$ as a function of the incident energy. The emission energy was selected using the $\langle 440 \rangle$ reflection of four spherically bent Ge crystal analyzers (with 1m bending radius) aligned at 80° Bragg angle. The intensity was normalized to the incident flux. The overall combined (incident convoluted with emitted) energy resolution of $\sim 0.4 \text{ eV}$ was obtained as determined by measuring the full width at half maximum (FWHM) of the elastic peak.

To measure the Se HERFD-XAS spectra the emission spectrometer was tuned to the top of the Se $K\alpha_1$ X-ray emission line ($\sim 11224 \text{ eV}$) and intensity was recorded as a function of the incident energy. The x-ray emission energy was selected using the $\langle 844 \rangle$ reflection of a Si crystal analyser aligned at 85° Bragg angle. The total

overall experimental resolution was estimated to be $\sim 1.9 \text{ eV}$.

The Ag L_3 - $M_{4,5}$ RIXS maps were recorded using a Johansson type in-vacuum tender x-ray emission spectrometer²². The spectrometer uses off-Rowland circle target position combined with position sensitive detection of x-rays. In our experiment, the sample was placed at a distance of 42 cm in front of the diffraction crystal, the first order reflection of the Si(111) crystal with 0.5 m Rowland circle radius was used, and the diffracted photons were detected by a thermoelectrically cooled (-40°C) CCD camera with $22.5 \times 22.5 \mu\text{m}^2$ pixel size.

III. COMPUTATIONAL DETAILS

The electronic structure was modelled using density functional theory as implemented in VASP (Vienna Ab initio Simulation Package) using pseudopotentials and the projector augmented-wave method for the basis set²³⁻²⁷.

The starting crystal structure²⁸ was taken from International Crystallographic Structural Database (ICSD)²⁹ (icsd no. 38309) and the geometry was relaxed in two steps. In the first step only the atoms were allowed to relax and in the second step only the volume was allowed to relax. For both cases the relaxation was stopped when the forces acting on each atom was less than 0.05 eV/\AA . The plane wave cut-off used was 250 eV (i.e. the largest default value for Ag, Mo and Se as provided in the VASP datasets). The k -point mesh was generated so that the distance between k -points was less than 0.14 \AA^{-1} in each reciprocal lattice vector direction. The electronic ground state was converged to $1\text{E-}6 \text{ eV}$.

The supercell included 18 Mo atoms, 22 Se atoms and 8 positions for four inequivalent Ag-atom types. The Ag1, Ag2, Ag3 and Ag4 notations, which we use in the present paper, correspond to those from Ref.²⁸. The preferential occupancy of different inequivalent Ag sites in $\text{Ag}_x\text{Mo}_9\text{Se}_{11}$ was taken into account in our calculations in accord with Ref.¹⁴ (see Supporting Information section) where the largest occupancy was found for the Ag1 sites and second large occupancy for Ag3 from the analysis of the x-ray diffraction data. The calculations were performed for the x values varying from 0.5 to 4.0 with the 0.5 step. On going from the $x = 3.0$ compound to the $x = 4.0$ compound, the increase in x in calculations was provided by populating only the Ag4 sites in accord with experimental data from Ref.¹⁴. Thus, the supercells for $x = 3.5$ and $x = 4.0$ in $\text{Ag}_x\text{Mo}_9\text{Se}_{11}$ contained 47 and 48 atoms, respectively. For $x = 3.5$, Ag populated 4 Ag1 (8f), 2 Ag3 (8f) and 1 Ag4 (16h) sites. For $x = 4.0$, 1 additional Ag4 (16h) site was populated. Since the Ag2 occupancy was found to be the smallest in $\text{Ag}_x\text{Mo}_9\text{Se}_{11}$ (Ref.¹⁴), it was entirely neglected in the calculations to avoid a further increase in the supercell size.

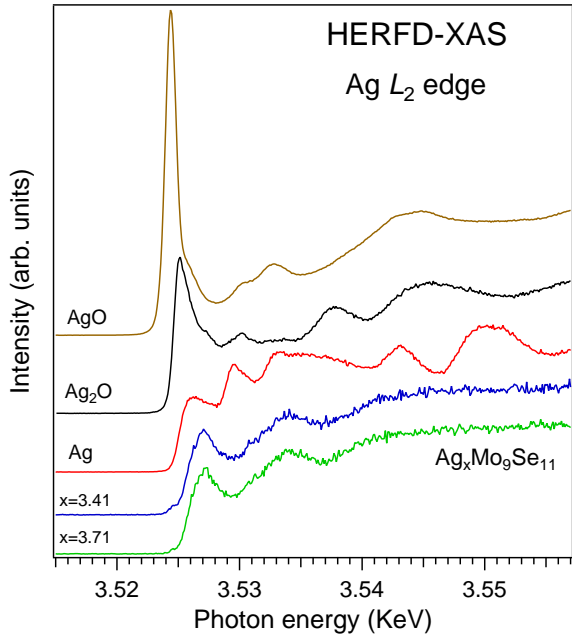


FIG. 1: X-ray absorption spectra recorded in the high energy resolution fluorescence detection mode (HERFD-XAS) at the Ag L_2 edge of Ag foil, Ag₂O, AgO and Ag_xMo₉Se₁₁ ($x=3.41$ or 3.71).

IV. RESULTS AND DISCUSSION

Fig. 1 displays the HERFD-XAS spectra recorded at the Ag L_2 edge of Ag foil, Ag₂O, AgO and Ag_xMo₉Se₁₁ ($x=3.41$ or 3.71). The spectra were normalized at ~ 3590 eV. The spectra appear narrower and with better resolved structures compared to the conventional XAS spectra (see the data for a number of reference Ag compounds in Refs.^{30–38}). This is because the HERFD-XAS technique leads to a reduction of the core-hole lifetime broadening of the spectra. In HERFD-XAS measurements at Ag $L_{2,3}$ edges, the $2p$ core hole (in the final state of conventional XAS) is replaced by the $3d$ core hole in the final state of the spectroscopic process. This results in significantly better resolution because the $3d$ core hole lifetime broadening (FWHM) is estimated to be ~ 0.3 eV³⁹ versus ~ 2.2 eV for the $2p$ core hole. Such an improvement for the XAS measurements at the Ag L_2 edge has been observed in Ref.⁴⁰.

At first glance, it seems that the Ag L_2 edge shifts to the low energy side when going from Ag metal to Ag₂O and to AgO. This behavior contrasts with the general behavior of the x-ray absorption edges with changing oxidation state of the transition element. Similar behavior is observed for the Cu $L_{2,3}$ edges, i.e. the shift to the low energy side when going from Cu(0) to Cu(I) and to Cu(II) compounds (see, for example, Refs.^{41–43} and references therein). However, Behrens *et al.*³² have argued for the case of Ag that the first peak (or white line) in the Ag L_3 XAS spectra of Ag₂O and to AgO develops as a results

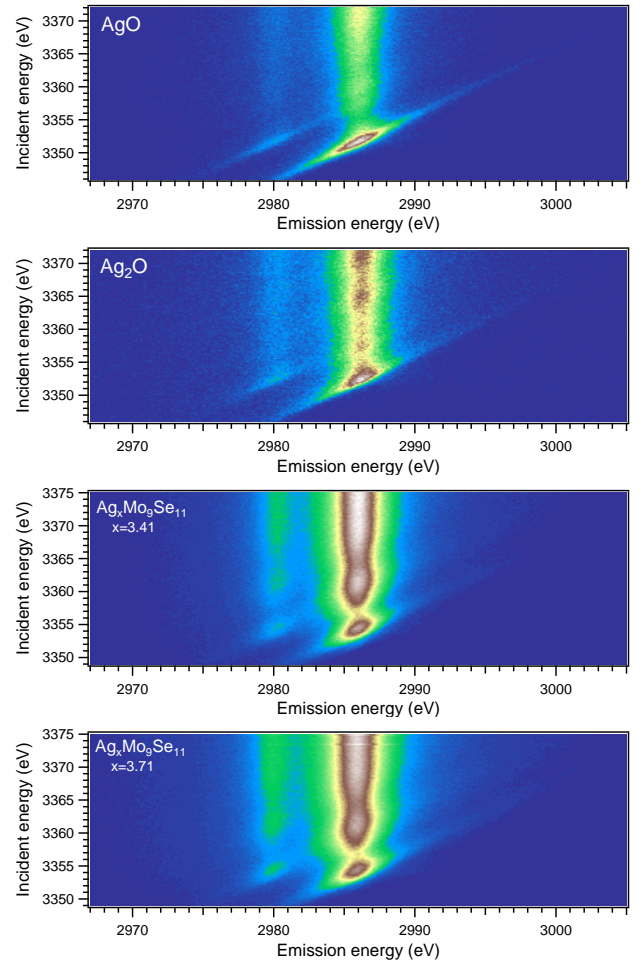


FIG. 2: Resonant inelastic x-ray scattering (RIXS) maps around Ag $L\alpha_1$ and $L\alpha_2$ x-ray emission lines of AgO, Ag₂O and Ag_xMo₉Se₁₁ ($x=3.41$ or 3.71).

of the appearance of the unoccupied Ag $4d$ states due to chemical bonding while for Ag metal, the first L_3 XAS structure has the $5s$ nature because the $4d$ is expected to be filled. Their conclusions have been supported by earlier band structure and XAS calculations³⁰ for Ag₂O. Behrens *et al.*³² have studied a number of Ag compounds and concluded that the intensity of the first Ag L_3 XAS structure/peak depends on the Ag oxidation state and degree of localization/delocalization of electronic states.

Miyamoto *et al.*³⁶ have performed measurements on a series of the Ag(I) compounds and found that the first Ag L_3 XAS structure is proportional to the degree of covalency in chemical bonding. In contrast to the conclusion of Ref.³², they have argued that this structure has the $5s$ origin. However, the latter statement is in contradiction with the reported results of various *ab-initio* calculations^{30,33,35,37} which indicate a significant contribution of the Ag $4d$ states to this structure. Furthermore, the calculations of the matrix elements for the Ag $2p-4d$ and $2p-5s$ transitions³³ as well as for the Cu $2p-3d$ and

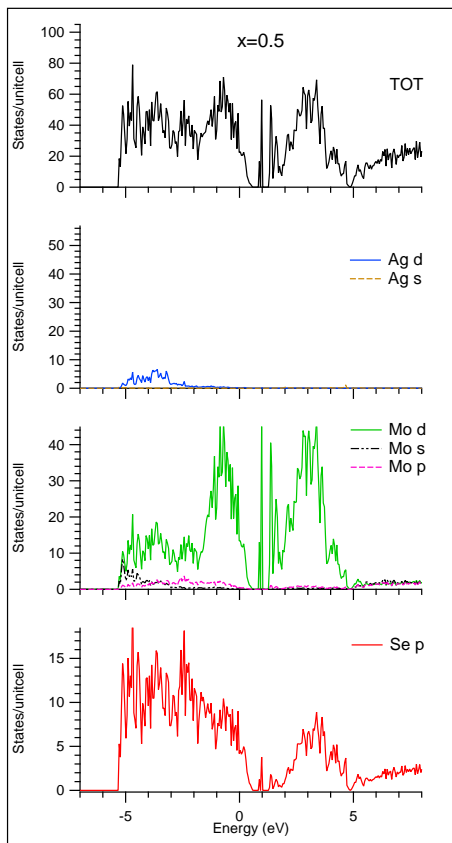


FIG. 3: Total and partial densities of states of $\text{Ag}_x\text{Mo}_9\text{Se}_{11}$ for $x = 0.5$. Only Ag1 sites assumed to be occupied. Zero eV corresponds to the position of the Fermi level.

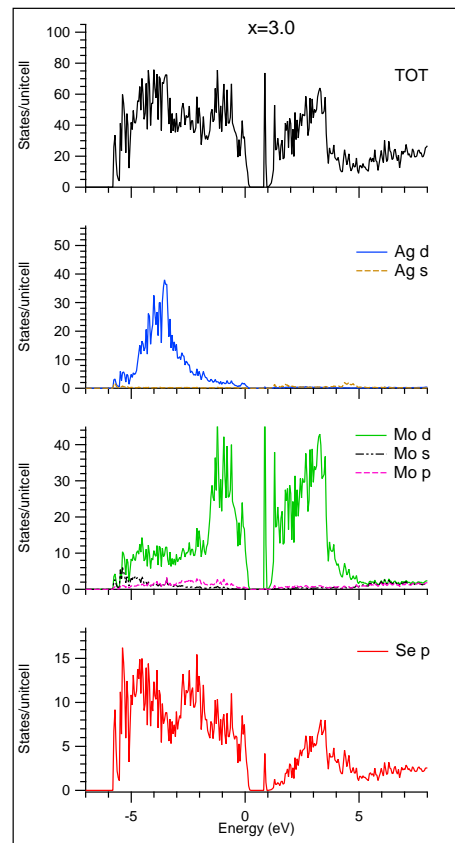


FIG. 4: Total and partial densities of states of $\text{Ag}_x\text{Mo}_9\text{Se}_{11}$ for $x = 3.0$. Zero eV corresponds to the position of the Fermi level.

$2p - 4s$ transitions⁴⁵ have obtained much smaller values for transitions to the s states. Bovenkamp³⁷ has pointed out the dependence of the energy position of the white line in the Ag L_3 XAS spectra of various Ag systems on the electronegativity of the atoms in the first coordination shell of the Ag atom. The white line maximum has been found to shift to higher energies with decreasing electronegativity of the neighboring atoms and based on comparison with FEFF calculations³⁷ it has been explained to be due to a shift of the Ag $4d$ contribution to the white line. The same considerations can be applied for the analysis of XAS spectra at the Ag L_2 edge.

While it has been assumed that Ag in the $\text{Ag}_x\text{Mo}_9\text{Se}_{11}$ system is in the Ag(I) state¹²⁻¹⁴, the results of our HERFD-XAS measurements reveal a more complex situation. Referring to the discussed above sensitivity of the white line to the Ag oxidation state and character of chemical bonding, the observed energy position and relative intensity of the Ag L_2 HERFD-XAS line at ~ 3527.5 eV of the $\text{Ag}_x\text{Mo}_9\text{Se}_{11}$ ($x=3.41$ or 3.71) samples, as compared to the lines in the spectra of Ag, Ag_2O and AgO , suggest a subvalent nature of the Ag atoms (less than $1+$) in the $\text{Ag}_x\text{Mo}_9\text{Se}_{11}$ system. An oxidation state lower than $1+$ indicates an incomplete charge transfer from the $5s$ and $4d$ electrons of Ag to the neighboring Se

atoms. Thus, these electrons rather belong to the $5s$ and $4d$ bands because of the degree of delocalization of the electronic states which is quite significant in comparison with Ag_2O and to AgO .

The degree of localization/delocalization of the electronic states can be also assessed from the core-to-core RIXS 2D-maps. Since such maps were not recorded during experiments at the Ag L_2 edge, they were obtained for the Ag L_3 edge using a Johansson type spectrometer²². Fig. 2 compares the RIXS maps measured around the Ag $L\alpha_{1,2}$ ($L_3\text{-}M_{4,5}$) x-ray emission lines for AgO , Ag_2O and $\text{Ag}_x\text{Mo}_9\text{Se}_{11}$ with $x=3.41$ and $x=3.71$, respectively. The resonating diagonal lines on these maps correspond to the RIXS component which has the constant energy loss for scattered photons and follows the increasing incident photon energy. The sharpness of such diagonal lines and the range of their extension on the incident photon energy scale is defined by the degree of the localization of the Ag $4d$ states participating in the $2p \rightarrow 4d$ excitation- $3d \rightarrow 2p$ deexcitation process. On going from AgO to Ag_2O and further to $\text{Ag}_x\text{Mo}_9\text{Se}_{11}$, these diagonal lines become more smeared out and less extended towards higher incident photon energies. Furthermore, in $\text{Ag}_x\text{Mo}_9\text{Se}_{11}$, most of the spectral intensity goes to the non-dispersive fluorescence-like line at the constant

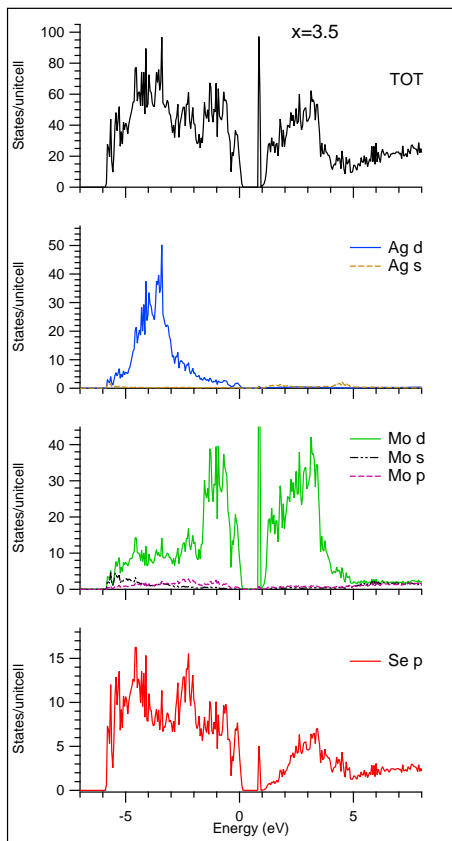


FIG. 5: Total and partial densities of states of $\text{Ag}_x\text{Mo}_9\text{Se}_{11}$ for $x = 3.5$. Zero eV corresponds to the position of the Fermi level.

emitted energy in comparison with AgO and Ag_2O . Such a behavior of the RIXS patterns also indicates that the Ag valence states in the $\text{Ag}_x\text{Mo}_9\text{Se}_{11}$ system are much more delocalized/itinerant compared to those in AgO and Ag_2O .

To examine the changes in the electronic structure of the $\text{Ag}_x\text{Mo}_9\text{Se}_{11}$ upon gradual Ag doping, the DFT calculations were performed for the x values varying from 0.5 to 4.0 with the 0.5 step. The calculated total and partial densities of states of $\text{Ag}_x\text{Mo}_9\text{Se}_{11}$ for some x values are displayed in Figs. 3-6. In agreement with calculations in Ref.¹⁴, our calculations indicate a metallic ground state for $x < 4.0$ while, for $x=4.0$, a semiconducting state with a band gap of 0.7 eV is reached. By comparing the results of calculations for various x , we can see that the Ag doping mostly affects the Se states in the valence band. This is not surprising because the Ag atoms are mainly introduced into the $\text{Mo}_9\text{Se}_{11}$ lattice voids close to the Se atoms^{12–14} leading to changes in the distribution of the Se states via hybridization with the Ag states in the valence band.

Taking into account some changes in the DOS and behavior of the Fermi level with increasing x , our calculations do not really support the validity of the rigid band model in the $\text{Ag}_x\text{Mo}_9\text{Se}_{11}$ system. Although, the shift of

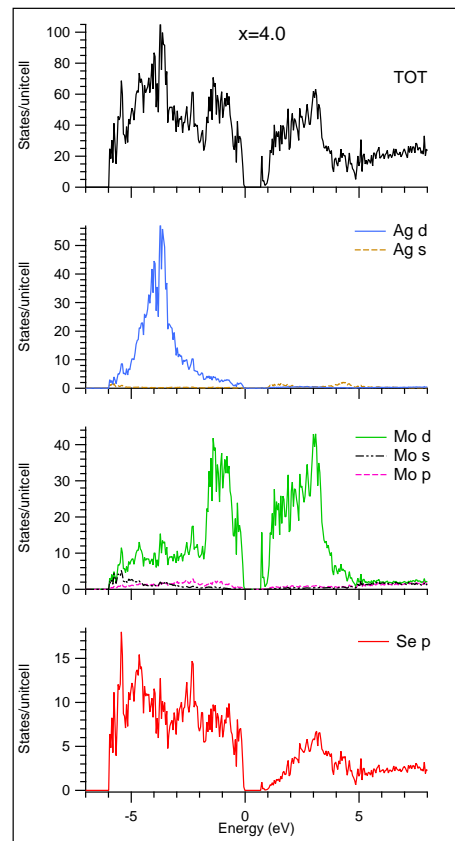


FIG. 6: Total and partial densities of states of $\text{Ag}_x\text{Mo}_9\text{Se}_{11}$ for $x = 4.0$. Zero eV corresponds to the position of the Fermi level.

the Fermi level seems to be gradual and proportional to the varying Ag content from $x = 0.5$ up to $x = 3.5$ (see Fig. 7), this shift suddenly shows a significant increase on going from $x = 3.5$ to $x = 4.0$. In the latter case, the shift is more than a half of the entire shift observed when x varies from $x = 0.5$ to $x = 3.5$.

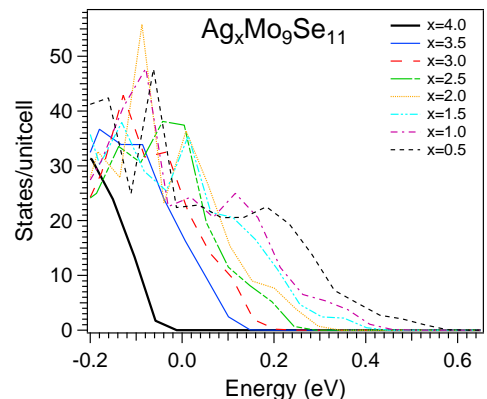


FIG. 7: Total densities of states of $\text{Ag}_x\text{Mo}_9\text{Se}_{11}$ for various x . Zero eV corresponds to the position of the Fermi level.

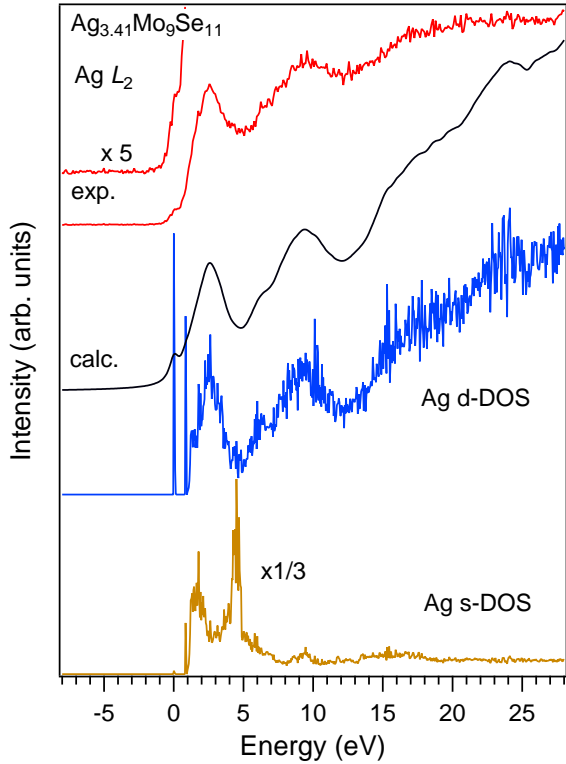


FIG. 8: Experimental Ag L_2 XAS spectrum of $\text{Ag}_{3.41}\text{Mo}_9\text{Se}_{11}$ compared to the calculated spectrum and unoccupied Ag d - and s -DOS of $\text{Ag}_{3.5}\text{Mo}_9\text{Se}_{11}$. The calculated spectrum is obtained by broadening the Ag d -DOS to account for experimental resolution.

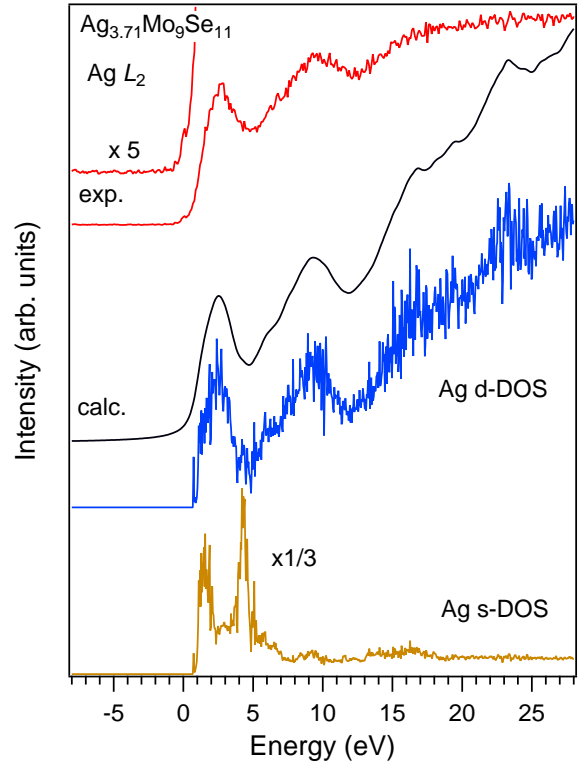


FIG. 9: Experimental Ag L_2 XAS spectrum of $\text{Ag}_{3.71}\text{Mo}_9\text{Se}_{11}$ compared to the calculated spectrum and unoccupied Ag d - and s -DOS of $\text{Ag}_{4.0}\text{Mo}_9\text{Se}_{11}$. The calculated spectrum is obtained by broadening the Ag d -DOS to account for experimental resolution.

A comparison of the broadened unoccupied DOS of Ag in $\text{Ag}_x\text{Mo}_9\text{Se}_{11}$ with HERFD-XAS spectra recorded at the Ag L_2 edge (Figs. 8, 9) shows that our calculations describe the experimental data fairly well. The HERFD-XAS spectra were brought onto the binding energy scale using the elastic peak in the valence-to-core RIXS spectra at the Ag L_2 edge and aligning the maximum of the Ag $L\gamma_1$ line with the gravity center of the occupied Ag $4d$ DOS. The results of the calculations reveal that all the structures in the Ag L_2 HERFD-XAS spectra are described well by the distribution of the unoccupied Ag d DOS. On the other hand, the major structures of the unoccupied Ag s DOS do not coincide with the spectral structures thus indicating significantly lower Ag s contribution to the measured spectra compared to the Ag d states, in accordance with conclusions about the matrix element ratio between the Ag $2p - 4d$ and $2p - 5s$ transitions in Ref.³³.

The first structure in the Ag L_2 HERFD-XAS spectra of $\text{Ag}_x\text{Mo}_9\text{Se}_{11}$ ($x=3.41$ and $x=3.71$) is observed at ~ 3524.5 eV (Fig. 1). This structure is fairly weak in $\text{Ag}_{3.71}\text{Mo}_9\text{Se}_{11}$ and somewhat stronger in $\text{Ag}_{3.41}\text{Mo}_9\text{Se}_{11}$. When the Ag L_2 HERFD-XAS spectra of $\text{Ag}_x\text{Mo}_9\text{Se}_{11}$ are brought to the binding energy scale (Figs. 8, 9), it becomes clear that their first structure cor-

responds to the contribution of the Ag states at the Fermi level. $\text{Ag}_{3.71}\text{Mo}_9\text{Se}_{11}$ is close to the $x=4.0$ composition with the predicted semiconducting behavior, therefore it is expected that the intensity of the first structure should be lower than that of $\text{Ag}_{3.41}\text{Mo}_9\text{Se}_{11}$.

Since the DFT calculations for $\text{Ag}_x\text{Mo}_9\text{Se}_{11}$ were performed with the 0.5 eV step in the varying x value, the measured spectra of $\text{Ag}_{3.41}\text{Mo}_9\text{Se}_{11}$ and $\text{Ag}_{3.71}\text{Mo}_9\text{Se}_{11}$ in Figs. 8-10 were compared with the results of the calculations for compositions close to those used in the measurements, i.e. $\text{Ag}_{3.5}\text{Mo}_9\text{Se}_{11}$ and $\text{Ag}_{4.0}\text{Mo}_9\text{Se}_{11}$, respectively. $\text{Ag}_{4.0}\text{Mo}_9\text{Se}_{11}$ is predicted to be a semiconductor by the calculations with the Fermi level positioned at the top of the valence band, therefore the first structure, corresponding to the contribution of the states at the Fermi level is entirely missing in the calculated XAS spectrum at the Ag $2p$ edge of $\text{Ag}_{4.0}\text{Mo}_9\text{Se}_{11}$ in comparison with a small peak at zero eV observed in the HERFD-XAS spectrum of $\text{Ag}_{3.71}\text{Mo}_9\text{Se}_{11}$. Otherwise, agreement between the experimental data and results of calculations in terms of the spectral shape for Ag in $\text{Ag}_x\text{Mo}_9\text{Se}_{11}$ is fairly good.

For Se in $\text{Ag}_x\text{Mo}_9\text{Se}_{11}$, the calculations also reproduce the differences in the shape of the main structures of the measured Se K edge between $\text{Ag}_{3.41}\text{Mo}_9\text{Se}_{11}$ and

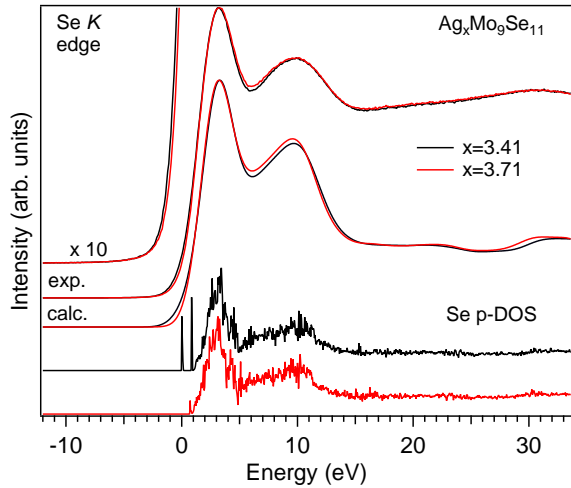


FIG. 10: Experimental Se K XAS spectra of $\text{Ag}_x\text{Mo}_9\text{Se}_{11}$ for $x=3.41$ and $x=3.71$ compared to calculated spectra and unoccupied Se p -DOS of $\text{Ag}_x\text{Mo}_9\text{Se}_{11}$ for $x=3.5$ and $x=4.0$, respectively.

$\text{Ag}_{3.71}\text{Mo}_9\text{Se}_{11}$ (see Fig. 10), in particular in the region of around 5-7 eV. The calculated unoccupied Se $4p$ DOS of $\text{Ag}_{3.5}\text{Mo}_9\text{Se}_{11}$ is peaking at the Fermi level and this gives rise to a clear enhancement of the intensity at zero eV of the calculated Se K XAS spectrum of the $x = 3.5$ compound compared to the $x = 4.0$ compound (Fig. 10). As in case of the Ag L_2 edge, the improved resolution of the HERFD-XAS spectra at the Se K edge allows one to observe the contribution of the Se $4p$ states at the Fermi level of $\text{Ag}_x\text{Mo}_9\text{Se}_{11}$ as a larger spectral weight around zero eV for $\text{Ag}_{3.41}\text{Mo}_9\text{Se}_{11}$ compared to $\text{Ag}_{3.71}\text{Mo}_9\text{Se}_{11}$.

Similar behavior of the unoccupied Ag and Se states at the Fermi level (i.e. degreasing contributions at E_F with increasing x) indicates the high degree of the delocalization of electronic states in the $\text{Ag}_x\text{Mo}_9\text{Se}_{11}$ system so that the electrons of Ag and Mo go to the band rather than participate in the ionic bonding with Se. A

comparison of the intensity of the structure at the Fermi level in the calculated and measured XAS spectra of $\text{Ag}_{3.41}\text{Mo}_9\text{Se}_{11}$ (Figs. 8, 10) shows that the calculations predict somewhat higher hole concentration than what is observed in experiment. A possible reason for such a difference could be a neglect of the finite occupancy of the Ag2 sites in $\text{Ag}_x\text{Mo}_9\text{Se}_{11}$ in the calculations. While the Ag2 occupancy is the smallest in comparison with Ag1, Ag3 and Ag4 sites (see Supporting Information section in Ref.¹⁴), the Ag2 atoms have the shortest Ag-Se distance²⁸ in $\text{Ag}_x\text{Mo}_9\text{Se}_{11}$. Therefore, this can be viewed as an indication of the Ag2 importance for affecting the properties of $\text{Ag}_x\text{Mo}_9\text{Se}_{11}$.

V. CONCLUSIONS

The use of the advanced x-ray spectroscopic technique, such as HERFD-XAS, allowed for resolving the important spectral structures at the Ag L_2 and Se K edges of $\text{Ag}_x\text{Mo}_9\text{Se}_{11}$ not observable in conventional XAS spectra. In particular, structures which represent the contributions of the unoccupied Ag and Se states at the Fermi level. The variation of these contributions with increasing x follows the trend predicted by the DFT calculations while our results show that a rigid-band approximation is not fully applicable in $\text{Ag}_x\text{Mo}_9\text{Se}_{11}$. Inserted Ag in $\text{Ag}_x\text{Mo}_9\text{Se}_{11}$ was found to be rather subvalent than in the Ag(I) state and the analysis of the data suggests the importance of the Ag2 atoms with the shortest Ag-Se distance for influencing the properties of $\text{Ag}_x\text{Mo}_9\text{Se}_{11}$.

VI. ACKNOWLEDGMENTS

We are grateful to the ID26 beamline staff for an excellent assistance with the preparation of the experiment. M.K., M.Ž. and K.B. acknowledge support from the Slovenian Ministry of Education, Science and Technology through the research program P1-0112.

¹ R. Chevrel, M. Sergent, J. Pringent, Sur de nouvelles phases sulfurées ternaires du molybdène. *J. Solid State Chem.*, 3 (1971) 515-519.
² Superconducting in Ternary Compounds; Fischer, Ø., Maple, M. B., Eds.; Springer-Verlag: Berlin, 1982; Parts I and II.
³ Petrović, AP; Lortz, R; Santi, G; Berthod, C; Dubois, C; Decroux, M; Demuer, A; Antunes, AB; Paré, A; Salloum, D; Gougeon, P; Potel, M; Fischer, Ø. Multiband Superconductivity in the Chevrel Phases SnMo_6S_8 and PbMo_6S_8 . *Phys. Rev. Lett.* 106 (2011) 017003.
⁴ Bergk, B; Petrović, AP; Wang, Z; Wang, Y; Salloum, D; Gougeon, P; Potel, M; Lortz, R. Superconducting transitions of intrinsic arrays of weakly coupled one-dimensional superconducting chains: the case of the extreme quasi-1D superconductor $\text{Tl}_2\text{Mo}_6\text{Se}_6$. *New J. Phys.* 13 (2011)

103018.

⁵ Petrović, AP; Ansermet, D; Chernyshov, D; Hoesch, M; Salloum, D; Gougeon, P; Potel, M; Boeri, L; Panagopoulos, C. A disorder-enhanced quasi-one-dimensional superconductor. *Nature Commun.* 7 (2016) 12262.
⁶ Ansermet, D; Petrović, AP; He, SK; Chernyshov, D; Hoesch, M; Salloum, D; Gougeon, P; Potel, M; Boeri, L; Andersen, OK; Panagopoulos, C. Reentrant Phase Coherence in Superconducting Nanowire Composites. *ACS Nano* 10 (2016) 515-523.
⁷ Q. Liu, A. Zunger, Predicted Realization of Cubic Dirac Fermion in Quasi-One-Dimensional Transition-Metal Monochalcogenides. *Phys. Rev. X* 7, 021019 (2017).
⁸ Picard, S.; Gougeon, P.; Potel, M. $\text{Rb}_{10}\text{Mo}_3\text{S}_{38}$: A Novel Reduced Molybdenum Sulfide Containing the Highest Nuclearity Metal Transition Cluster in a Solid-State Com-

- pound. *Angew. Chem., Int. Ed.* 1999, 38, 2034-2036.
- 9 T. Caillat, J.-P. Fleurial, G. J. Snyder, Potential of Chevrel phases for thermoelectric applications. *Solid State Sci.* 1, 1999, p. 535-544.
 - 10 Gougeon, P.; Gall, P.; Al Orabi, RA; Fontaine, B; Gautier, R; Potel, M; Zhou, T; Lenoir, B; Colin, M; Candolfi, C; Dauscher, A. Synthesis, Crystal and Electronic Structures, and Thermoelectric Properties of the Novel Cluster Compound $\text{Ag}_3\text{In}_2\text{Mo}_{15}\text{Se}_{19}$. *Chem. Mater.* 24 (2012) 2899-2908.
 - 11 R. Al Rahal Al Orabi, P. Gougeon, P. Gall, B. Fontaine, R. Gautier, M. Colin, C. Candolfi, A. Dauscher, J. Hejtmanek, B. Malaman, B. Lenoir, X-ray Characterization, Electronic Band Structure, and Thermoelectric Properties of the Cluster Compound $\text{Ag}_2\text{Tl}_2\text{Mo}_9\text{Se}_{11}$. *Inorg. Chem.*, 2014, 53 (21), 1169911709.
 - 12 Zhou, T; Lenoir, B; Colin, M; Dauscher, A; Al Orabi, RA; Gougeon, P; Potel, M; Guilmeau, E. Promising thermoelectric properties in $\text{Ag}_x\text{Mo}_9\text{Se}_{11}$ compounds ($3.4 \leq x \leq 3.9$). *Applied Phys. Lett.* 98(16) (2011) 162106.
 - 13 Zhou, T; Lenoir, B; Christophe, C; Dauscher, A; Gall, P; Gougeon, P; Potel, M; Guilmeau, E. Cage-Shaped Mo-9 Chalcogenides: Promising Thermoelectric Materials with Significantly Low Thermal Conductivity. *J. Electronic Mater.* 40(5) (2011) 508-512.
 - 14 Zhou, T; Colin, M; Candolfi, C ; Boulanger, C ; Dauscher, A; Santava, E; Hejtmanek, J; Baranek, P; Al Orabi, RA; Potel, M; Fontaine, B; Gougeon, P; Gautier, R; Lenoir, B. Comprehensive Study of the Low-Temperature Transport and Thermodynamic Properties of the Cluster Compounds $\text{Ag}_x\text{Mo}_9\text{Se}_{11}$ ($3.41 \leq x \leq 3.78$). *Chem. Mater.* 26(16) (2014) 4765-4775.
 - 15 Stern, E. A. Rigid band model of alloys. *Phys. Rev.* 157, 544-551 (1967).
 - 16 Mal-Soon Lee, S. D. Mahanti, Validity of the rigid band approximation in the study of the thermopower of narrow band gap semiconductors. *Phys. Rev. B* 2012, 85, 165149.
 - 17 D. Kasinathan, M. Wagner, K. Koepernik, R. Cardoso-Gil, Yu. Grin, H. Rosner, Electronic and thermoelectric properties of $\text{RuIn}_{3-x}\text{A}_x$ ($\text{A} = \text{Sn}, \text{Zn}$). *Phys. Rev. B* 2012, 85, 035207.
 - 18 Y. Takagiwa, Y. Pei, G. Pomrehn, G. J. Snyder, Validity of rigid band approximation of PbTe thermoelectric materials. *APL Materials* 1, 011101 (2013).
 - 19 Y. Suzuki, H. Nakamura, A supercell approach to the doping effect on the thermoelectric properties of SnSe. *Phys.Chem.Chem.Phys.*, 2015, 17, 29647-29654.
 - 20 Gauthier C, Sole VA, Signorato R, Goulon J, Mognuine E (1999) The ESRF beamline ID26: X-ray absorption on ultra dilute sample. *J. Synchrotron Radiat.* 6:164-166.
 - 21 Glatzel P, Bergmann U (2005) High Resolution 1s Core Hole X-ray Spectroscopy in 3d Transition Metal Complexes: Electronic and Structural Information. *Coordin. Chem. Rev.* 249:65-95.
 - 22 M. Kavčič, M. Budnar, A. Mühleisen, F. Gasser, M. Žitnik, K. Bučar, R. Bohinc, *Rev. Sci. Instrum.* 83, 033113 (2012).
 - 23 W. Kohn and L. J. Sham, Self-Consistent Equations Including Exchange and Correlation Effects, *Phys. Rev.* 140, A1133 (1965).
 - 24 G. Kresse and J. Furthmuller, Efficient Iterative Schemes for Ab Initio Total-Energy Calculations Using a Plane-Wave Basis Set, *Phys. Rev. B* 54, 11169 (1996).
 - 25 G. Kresse and D. Joubert, From Ultrasoft Pseudopotentials to the Projector Augmented-Wave Method, *Phys. Rev. B* 59, 1758 (1999).
 - 26 J. P. Perdew, J. A. Chevary, S.H. Vosko, K. A. Jackson, M. R. Pederson, D. J. Singh, and C. Fiolhais, Atoms, Molecules, Solids, and Surfaces: Applications of the Generalized Gradient Approximation for Exchange and Correlation, *Phys. Rev. B* 46, 6671 (1992); Erratum *Phys. Rev. B* 48, 4978 (1993)
 - 27 P. E. Blchl, Projector Augmented-Wave Method, *Phys. Rev. B* 50, 17953 (1994).
 - 28 P. Gougeon, J. Padiou, J. Y. Le Marouille, M. Potel, M. Sergent, $\text{Ag}_{3.6}\text{Mo}_9\text{Se}_{11}$: Premier composé à clusters Mo_9 dans des motifs $\text{Mo}_9\text{Se}_{11}$. *J. Solid State Chem.* 1984, 51, 218-226.
 - 29 <https://icsd.fiz-karlsruhe.de>
 - 30 Czyżyk, M. T.; de Groot, R. A.; Dalba, G.; Fornasini, P.; Kisiel, A.; Rocca, F.; Burattini, E. Ag_2O band structure and x-ray absorption near-edge spectra. *Phys. Rev. B* 1989, 39, 9831-9838.
 - 31 Behrens, P. Bonding in silver-oxygen compounds from $\text{Ag } L_3$ XANES spectroscopy. *Solid State Commun.* 1992, 81, 235-239.
 - 32 Behrens, P.; Abmann, S.; Bilow, U.; Linke, C.; Jansen, M. Z. Electronic Structure of Silver Oxides Investigated by $\text{Ag } L$ XANES Spectroscopy. *Anorg. Allg. Chem.* 1999, 625, 111.
 - 33 Sivr, O.; Rocca, F.; Dalba, G. Real-space multiple-scattering analysis of $\text{Ag } L_{1-}$ and L_3 -edge XANES spectra of Ag_2O . *J. Synchrotron Rad.* (1999). 6, 770-772.
 - 34 A. V. Kolobov, A. Rogalev, F. Wilhelm, N. Jaouen, T. Shima, J. Tominaga, Thermal decomposition of a thin AgO_x layer generating optical near-field. *Appl. Phys. Lett.* 84, 1641-1643 (2004).
 - 35 U. Wedig, P. Adler, J. Nuss, H. Modrowb, M. Jansen, Studies on the electronic structure of Ag_2NiO_2 , an intercalated delafossite containing subvalent silver. *Solid State Sci.* 8 (2006) 753763.
 - 36 T. Miyamoto, H. Niimi, Y. Kitajima, T. Naito, K. Asakura, $\text{Ag } L_3$ -Edge X-ray Absorption Near-Edge Structure of $4d^{10}$ (Ag^+) Compounds: Origin of the Edge Peak and Its Chemical Relevance. *J. Phys. Chem. A* 2010, 114, 4093-4098.
 - 37 G. L. Bovenkamp, X-Ray Absorption Spectroscopy in Biological Systems: Opportunities and Limitations. PhD thesis, Physikalisches Institut, Universität Bonn, ISSN 0172-8741, 2013.
 - 38 Y. A. Attia, D. Buceta, F. G. Requejo, L. J. Giovanettid, M. A. López-Quintela, Photostability of gold nanoparticles with different shapes: the role of Ag clusters. *Nanoscale*, 2015, 7, 11273-11279.
 - 39 J. L. Campbell, T. Papp, Widths of the Atomic K-N₇ Levels. *Atomic Data and Nuclear Data Tables* 77, 156 (2001).
 - 40 E. Coutino-Gonzalez, D. Grandjean, M. Roeffaers, K. Kvashnina, E. Fron, B. Dieu, G. De Cremer, P. Lievens, B Sels, J. Hofkens, X-ray irradiation-induced formation of luminescent silver clusters in nanoporous matrices. *Chem. Commun.*, 2014, 50, 1350-1352.
 - 41 J. R. Vegelius, K. O. Kvashnina, H. Hollmark, M. Klintenber, Y. O. Kvashnin, I. L. Soroka, L. Werme, S. M. Butorin, X-ray Spectroscopic Study of Cu_2S , CuS , and Copper Films Exposed to Na_2S Solutions. *J. Phys. Chem. C* 2012, 116, 22293-22300.
 - 42 K.O. Kvashnina, S.M. Butorin, A. Modin, L. Werme, J. Nordgren, J.-H. Guo, R. Berger, L. Werme and J. Nordgren, Electronic structure of complex copper systems

- probed by resonant inelastic x-ray scattering at Cu L_3 edge. *Physica B* 404, 3559 (2009).
- ⁴³ K.O. Kvashnina, S. M. Butorin, A. Modin, I. Soroka, M. Marsellini, J.-H. Guo, L. Werme, and J. Nordgren, Changes in electronic structure of copper films in aqueous solutions. *J. Phys: Condens. Matter* 19, 13 (2007).
- ⁴⁴ J. R. Vegelius, K. O. Kvashnina, M. Klintonberg, I. L. Soroka, S. M. Butorin, Cu $K\beta_{2,5}$ X-ray emission spectroscopy as a tool for characterization of monovalent copper compounds. *J. Anal. At. Spectrom.*, 2012, 27, 1882-1888.
- ⁴⁵ O. Bunău, M. Calandra, Projector augmented wave calculation of x-ray absorption spectra at the $L_{2,3}$ edges. *Phys. Rev. B* 87, 205105 (2013).